Design, Modeling, and Evaluation of a Multiband MIMO/Diversity Antenna System for Small Wireless Mobile Terminals

Qinjiang Rao and Kelce Wilson

***Abstract*—A new multiband diversity antenna is presented, which is suitable for multiband diversity and multiple–input multiple–output antenna systems for small wireless mobile terminals. The antenna consists of two branches of folded monopoles, at least one of which is terminated with a rectangular patch. By slightly tuning the width of the patch, the antenna can simultaneously achieve a flexible frequency ratio and a desired bandwidth. An example design is presented for most application bands, from 890 MHz through 6 GHz, which operates in a real-world cellular phone environment, including near-field interactions with other phone components and a model of a human head (the SAM phantom). The simulated and experimental results, including *S*-parameters, radiation patterns, signal correlations and mean effective gain, have validated the proposed antenna design as useful for compact mobile devices.**

***Index Terms*—Antenna diversity, antenna efficiency, mean effective gain, signal correlation coefficient.**

I. Introduction

WIRELESS communication systems are widely deployed to provide a broad range of voice and data-related services. Typical wireless communication systems consist of multiple-access communication networks that allow users of wireless mobile devices to share common network resources. These networks typically require multiband antennas for transmitting and receiving radio-frequency (RF) signals from wireless devices. Recent demand for increased data capacity has driven the development of multi-antenna systems for wireless mobile devices, such as cellular phone handsets. Multiple–input multiple–output (MIMO) and diversity systems are potential technologies for enhancing performance with high-speed transmission rates [1]–[10].

In order to achieve the desired performance of a multi-antenna system, such as a long term evolution (LTE) MIMO or other diversity system, in a tightly volume-constrained device, several technical obstacles must be overcome. One of these obstacles is mutual coupling of closely-spaced antennas, as is common in cellular phone handsets. Higher levels of mutual coupling, which can easily occur in handset MIMO systems, can significantly degrade antenna efficiencies, as well as produce undesirable signal correlation between multiple antenna outputs. High signal correlation is associated with the loss of spectral efficiency and can degrade MIMO system throughput and battery efficiency. Therefore, to achieve the desired low signal correlation, MIMO systems require high diversity and reduced coupling, which is also identified as a high port-to-port isolation.

A common approach for achieving the required low signal correlation and high port isolation is widely separating the antennas. Unfortunately, the approach of relying on physical separation of the antennas is not feasible for many compact handheld devices, because the volume that must be dedicated to a MIMO antenna system can become prohibitively large. This coupling problem can become acute as the number of antennas increases. Therefore, since compact handheld devices may lack the size necessary to permit adequate inter-antenna spacing, multi-antenna systems in compact handheld devices may often experience undesirable signal correlation that noticeably degrades MIMO performance.

Thus, designers of antenna systems for mobile devices face significant challenges, particularly when the antenna elements in a multi-antenna system such as MIMO must be capable of covering several differing bands while fitting within tight volumes, providing high diversity performance, and achieving reasonable mean effective gain (MEG) across all bands of operation. In addition, it is desirable for the antenna systems to be inexpensive and easily manufactured for installation in a wireless device.

This paper presents a new multiband, dual-element diversity antenna system, which is suitable for compact multimode wireless handheld devices. The proposed system operates over an exceptionally broad bandwidth, from 890 MHz to 6 GHz [11]. In order to validate the practicality of the proposed system, the antenna design is tested in real-world environments, similar to those in which compact wireless handheld devices are expected to operate. The near-field environments are created using the housing and enclosed circuitry of a production-style Blackberry 8900 Bold model smart phone. The major components that provide the near-field electromagnetic interaction with the antennas include a liquid crystal display (LCD), a battery, a dielectric frame, and an exterior plastic shell. Additionally, the proposed design takes into account the potentially performance-degrading interactions between an antenna system and a human head in close proximity.

Manuscript received March 26, 2010; revised June 20, 2010; accepted September 02, 2010. Date of publication December 23, 2010; date of current version April 08, 2011. This work was recommended for publication by Associate Editor L.-T. Hwang upon evaluation of the reviewers comments.

The authors are with Research In Motion, Waterloo, ON, N2L 5Z5 Canada (e-mail: qirao@rim.com; kewilson@rim.com).

Digital Object Identifier 10.1109/TCPMT.2010.2101234

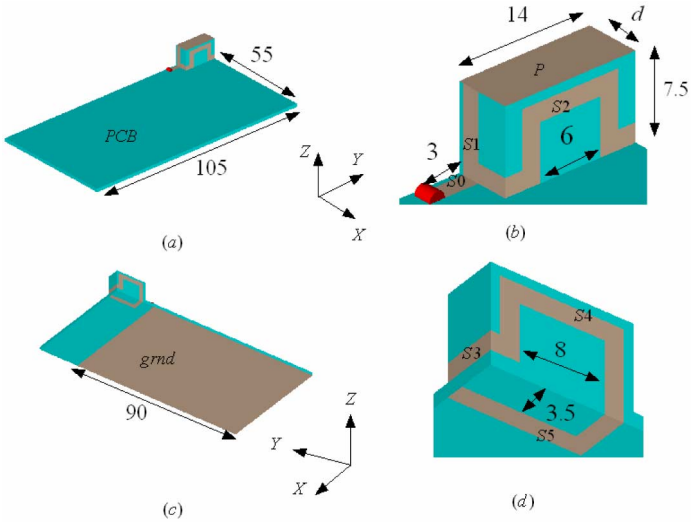

Fig. 1. The configuration of the proposed antenna. (Unit: mm). All strips have an identical width of 2 mm. (a) and (c): Folded strip antenna on a PCB of 10.5 cm×5.5 cm. (b) and (d): Enlarged 3-D view of the strip antenna.

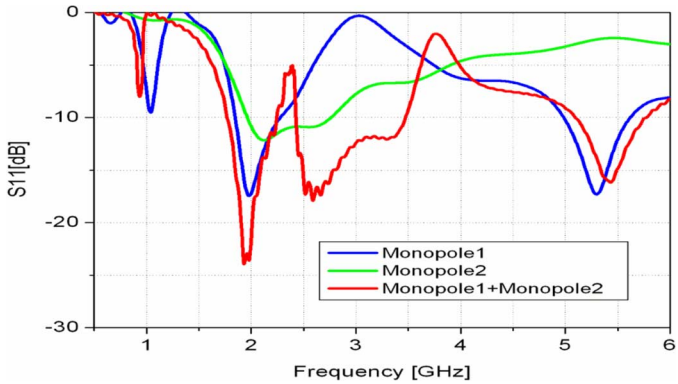

Fig. 2. Comparison of simulated reflection coefficients $S11$.

Both simulated and experimental results are reported, including S-parameter, radiation pattern, signal correlation, and MEG. The results suggest that the proposed design has significant potential for current and future wireless devices, including multiband MIMO antennas for smart-phones.

Section II describes the layout and fundamental features of the proposed antenna system. Section III describes the implementation of a dual-element diversity structure in a real-world smart-phone environment, along with the operational characteristics. Finally, Section IV briefly summarizes the results.

II. Multiband Antenna

A new multiband monopole antenna is presented, which can cover almost all cellular relevant bands, from 890 MHz to 6 GHz. One unique approach used in the proposed design, which permits tuning while retaining a small antenna size, is use of several radiation strips of various lengths, with a rectangular conducting patch terminating the shorter branch. Slight adjustments to the width of the patch can result in significant tuning of bandwidth and resonating frequency, without changing the overall size of the antenna.

A. Antenna Structure

Fig. 1 shows the configuration of the proposed antenna. The antenna consists of a rectangular ground plane, a rectangular metal patch P and two branches of monopoles composed of multiple metal strips ($S0$, $S1$, $S2$, $S3$, $S4$, and $S5$), each with the identical width of 2 mm. As the fractional bandwidth of an antenna is approximately the inverse of its Q [12], and bending a metal antenna to permit it to efficiently occupy a small volume can reduce its Q [12], [13], a folded 3-D monopole enjoys simultaneous benefits: enhanced bandwidth and smaller required volume.

Since the size and shape of a GP can impact antenna performance, it must be included in the simulation and testing. For the proposed design, the ground plane (GP) is set to a size of 5.5 cm×10.5 cm. A conductor is placed on the surface of a substrate, which has a thickness of 1.5 mm and a relative dielectric constant of 4.4. A dielectric shell with a thickness of 1 mm, and a relative dielectric constant also of 4.4, is used to support the conductive strips of the antenna, and its dimensions are 0.7 cm × 1.5 cm × 0.75 cm. During the design phase, it was discovered that removing a 1.5 cm × 5.5 cm portion of the conductor from the GP nearby the antenna provided approximately omni-directional radiations and enhanced impedance matching over a rather broad frequency range.

For this antenna, the conductive strips are primary radiation elements, and constitute two monopole radiators, identified here as monopole 1 and monopole 2. Monopole 1 is composed of $S0$, the horizontal portion of $S1$ (as illustrated), $S2$, $S3$, $S4$, and $S5$. Monopole 2 is composed of $S0$, the vertical portion of $S1$ and patch P. Since the total length and layout of each monopole determines the antenna's performance, these strips must be optimized within the constraints of allowable antenna volume and the desired resonant frequency. The initial design goal is to set the electrical length of monopole 1 to a quarter of the wavelength at the fundamental mode of 1 GHz and the electrical length of monopole 2 to a quarter of the wavelength at the fundamental mode of 2 GHz.

The initial geometric parameters were optimized by using CST [14], a commercial electromagnetic simulator based on FDTD and the obtained values are shown in Fig. 1. Strips $S2$, $S3$, and $S4$ are the three U-shaped strips, $S1$ and $S5$ are the two L-shaped strips. The width d of patch P plays a critical role in determining the bandwidth. The value of d was varied to study the effects on antenna performance. In the initial design, the width d was set at 2 mm, identical to the other strips. With this arrangement, the two monopoles are folded onto the shell and fed through the shared conductor $S0$.

B. Resonant Frequency

Fig. 2 shows a comparison of the three simulated reflection coefficients: 1) monopole 1 excited only, 2) monopole 2 excited only, and 3) both monopole 1 and monopole 2 excited simultaneously. These curves indicate the resonant frequencies of the initial structure, illustrated in Fig. 1.

As can be seen in Fig. 2, when monopole 1 is excited alone, the antenna resonates at three different frequencies: 1, 2, and 5.45 GHz. The frequency ratio is 2:1 for the second-order

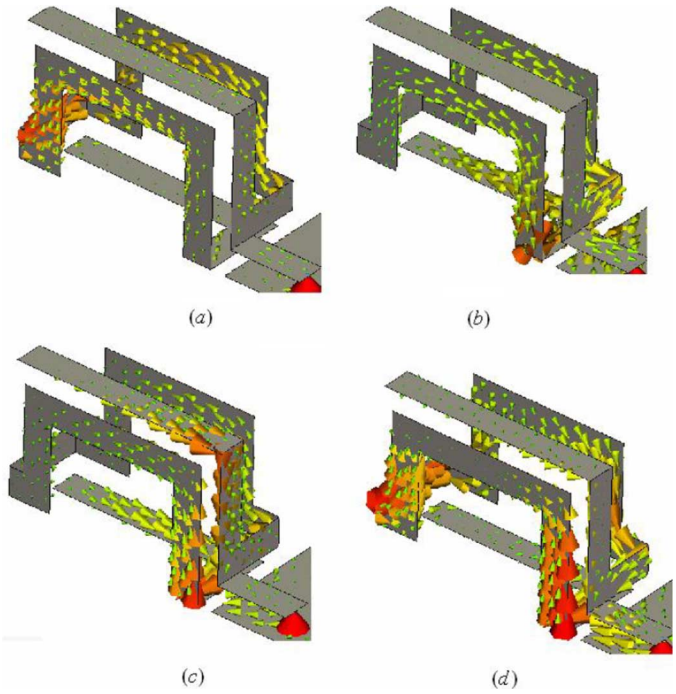

Fig. 3. Simulated electric current distributions on the monopole 1 and monopole 2 at different resonant frequencies while they are excited at the same time. (a) 900 MHz. (b) 2.2 GHz. (c) 2.5 GHz. (d) 5.45 GHz.

mode to the dominant mode. Unfortunately, the bandwidth at the 2 GHz region is not wide enough to cover all current application bands, such as GSM1800/1900, UMTS 2100, and the WLAN 2.4 GHz band.

When monopole 2 is excited alone, it has only the fundamental mode resonant frequency at 2.5 GHz. Although the impedance bandwidth, defined by a 10 dB return loss, is wider for monopole 2 than for monopole 1, it is still not sufficient to cover all needed application bands. However, when the two monopoles are excited simultaneously, the antenna offers four resonant frequencies of 0.95, 2, 2.5, and 5.4 GHz. Compared to the *S*11 parameters, obtained by separately exciting monopole 1 and monopole 2, the bandwidths and impedance matching at 0.95, 2, and 5.4 GHz bands have only very slight changes. However, the bandwidth at 2.5 GHz band is significantly enhanced. Thus, we can conclude that monopole 1 is the primary driver of the bandwidths and resonances at 0.95, 2, and 5.4 GHz, while monopole 2 is the primary driver of the bandwidth at 2.5 GHz.

C. Current Distribution

In order to enhance understanding of the multiband operation, current distributions on the two monopoles are simulated and investigated.

Fig. 3 shows the current distributions on both monopoles at various frequencies when they are excited simultaneously. Within the frequency bands of 1, 2, and 5.5 GHz, monopole 1 has strong surface currents, whereas monopole 2 has only weak currents. This indicates that the two monopoles have high mode, isolation, and monopole 1 is the one that mostly determines these resonant frequencies. However, when the antenna operates at 2.5 GHz, both monopoles deploy strong currents, so they both affect performance at 2.5 GHz.

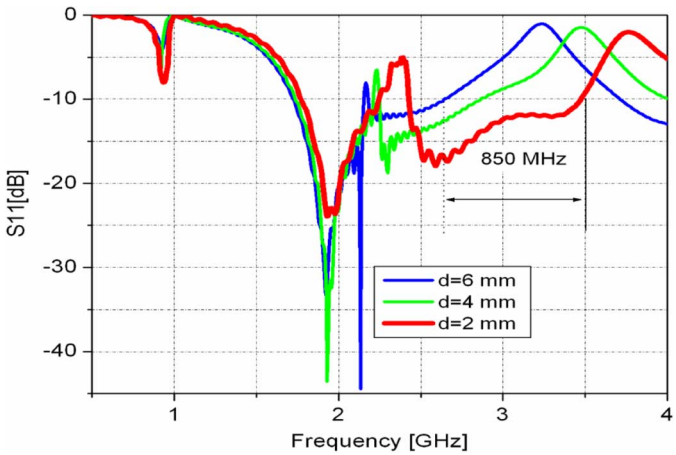

Fig. 4. Effects of the width d of the patch *P* on reflection coefficient *S*11.

D. Impact of Loading Patch

Next, the influence of patch *P* on the antenna performance is examined. Fig. 4 shows that the width *d* of patch *P* significantly affects resonant frequency and bandwidth in the range of 2.2 to 4 GHz, but it has almost no influence at frequencies below 2 GHz, except for a slight change to impedance matching. This is expected, based on the high mode-isolation noted in the previous section. With the high mode-isolation now verified, we can independently tailor the lower and the upper bands of monopole 1 and monopole 2. Another important interpretation of Fig. 4 is that by slightly adjusting width *d*, from 2 to 6 mm, the antenna provides a number of desired frequency bands within a flexible resonant frequency range from 2 to 4 GHz. These covers almost all current and planned future application bands at GSM 1800/1900, UMTS2100, Blue-tooth 2.4 GHz, WiFi/LTE 2.6 GHz, and WiMAX 3.3–3.8 GHz. One potential application is the use of RF switches, such as RF micro- electro mechanical systems (RF-MEMS), to reconfigure patch *P* so that the antenna provides greater flexibility and frequency agility

III. Multiband Dual-Element Diversity Antenna

Based on the antenna element presented in the previous section, a multiband dual-diversity antenna system is designed and implemented in a real-world smartphone housing.

Fig. 5 shows two elements integrated into a real-world smartphone environment. The two elements are of identical size, the same as described previously. They are oriented orthogonally, for diversity performance. There is a rectangular stub between the two array elements, which is used as a ground plane for the excitation of antenna 2. Adjusting the dimensions of the stub affects impedance matching, antenna coupling, operational frequencies and radiation patterns. The size used for this study is 5 mm×13 mm.

Fig. 5 illustrates a typical hand-held geometric model, which is based on the near field environments of a production device: the Blackberry 8900 Bold smartphone. This device has a maximum form factor of 100 mm × 55 mm × 13.5 mm. Major electromechanical components include the dual-port radiation elements, a frame for supporting the antenna, a PCB, a plastic

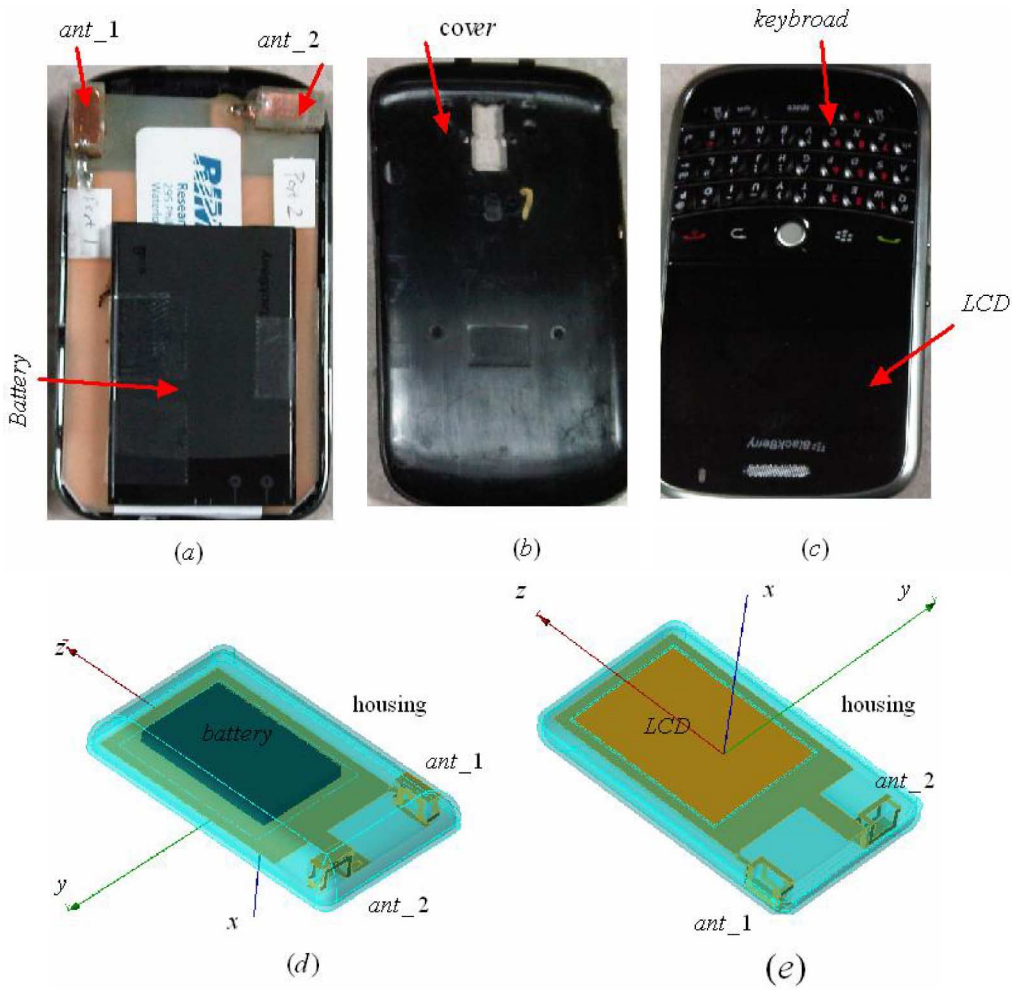

Fig. 5. The dual-antennas are prototyped in real device enviroments and related to the simulation model.

housing, an LCD (52 mm × 63.2 mm × 2 mm), and a battery (33.5 mm × 50.5 mm × 4.5 mm). The LCD, battery and ground plane were modeled as metal materials, whereas the frame and plastic cover were modeled as dielectric materials. The dielectric constants used for the frame and the cover were $\varepsilon_r = 2.2$ and $\varepsilon_r = 4.4$, respectively.

A. Return Loss and Isolation

Fig. 6 illustrates a comparison of the simulated and measured *S*-parameters as a function of frequency for the handset device in free space. The agreement is generally good. It can be seen in Fig. 6 that good isolation performance and impedance matching characteristics have been achieved. The dual-antenna system functions at multiple bands, ranging from 890 MHz to 6 GHz, with isolation better than 10 dB across all bands. These values indicate that the two diversity antenna elements are highly isolated, even though they are only separated by a distance of 17.5 mm. This separation distance is a mere 0.05 free space wavelength at 890 MHz. The excellent isolation may be due to the fact that the primary current intensity is confined to the folded strip areas, and less is on the ground plane. Additionally, the two branch radiation elements are oriented orthogonally to each other, which can achieve excellent orthogonal polarization and pattern diversity that would be helpful for achieving high isolation.

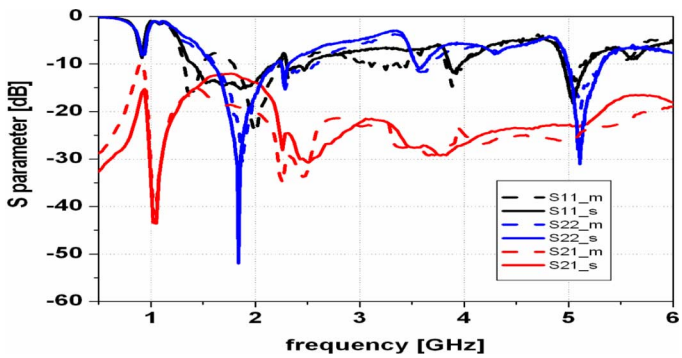

Fig. 6. Simulation and measured *S*-parameters.

B. Radiation Patterns

The radiation 3-D gain patterns were simulated by GEMS [15], a commercial EM simulator based on FDTD, and measured by a near-field test system provided by Satimo [16]. When one port was excited, the other was terminated with a 50 Ω

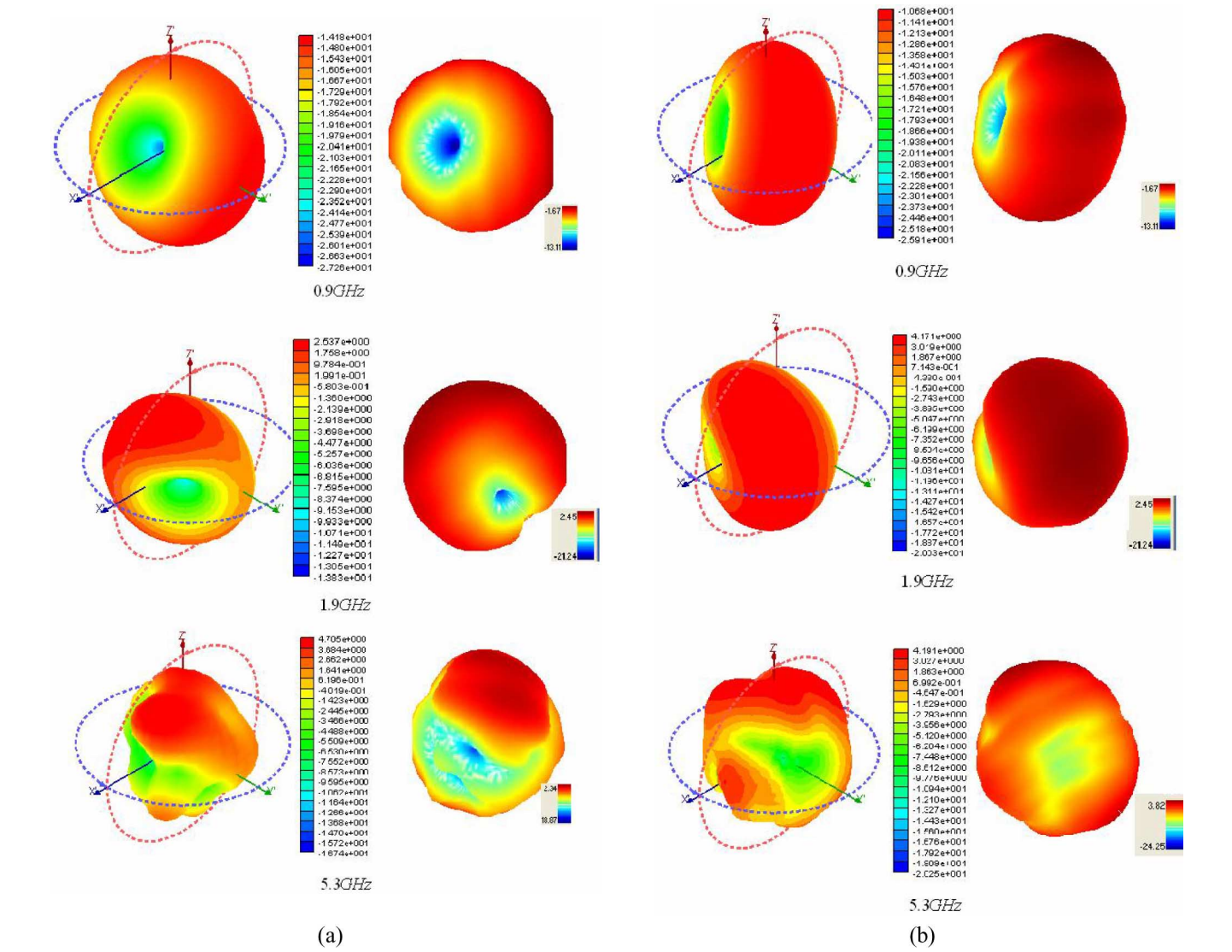

Fig. 7. Simulated (L) and measured (R) gain patterns at (a) port1 and (b) port2.

matching load. Fig. 7(a) and (b) illustrates results for several typical operating frequencies: 900 MHz, 1.9 GHz, and 5.3 GHz, at ports 1 and 2, respectively. It can be seen that the simulated and measured patterns are generally in good agreement, and the two antennas display good pattern diversity in both simulations and measurements.

Fig. 8 plots the simulated 2-D radiation patterns at several frequencies: 900 MHz, 1.9 GHz, 2.45 GHz, 2.7 GHz, and 5.5 GHz. The radiation patterns for the antennas cover complimentary space regions, providing good pattern diversity, especially in the X–Y plane.

C. Diversity Performance

Two figures of merit for a multi-antenna system performance are the MEG and the envelope correlation coefficient (ECC). The MEG is a statistical measure of the antenna gain in a given operational environment. It defines the power received by an antenna, accounting for the effects of the radiation power pattern, the antenna total efficiency, and the propagation effects as in the following equation [17]:

$$\mathrm{MEG} = \eta_{\mathrm{total}} \int_0^{2\pi} \int_0^{\pi} \left(\frac{\mathrm{XPR}}{1+\mathrm{XPR}} G_\theta(\theta,\phi) P_\theta(\theta,\phi) + \frac{1}{1+\mathrm{XPR}} G_\phi(\theta,\phi) P_\phi(\theta,\phi) \sin\theta \, d\theta \, d\phi \right) \tag{1}$$

$$\int_0^{2\pi} \int_0^{\pi} (G_\theta(\theta,\phi) P_\theta(\theta,\phi) + G_\phi(\theta,\phi) P_\phi(\theta,\phi) \sin\theta \, d\theta \, d\phi) = 4\pi \tag{2}$$

where P_θ and P_ϕ are the angular density functions of the incident power; XPR represents the cross-polarization discrimination; and G_θ and G_ϕ are the θ- and φ-polarized components of the antenna power gain patterns, respectively. The density functions are different for differing distributions. We have used common distributions, for example Gaussian, LaPlacian,

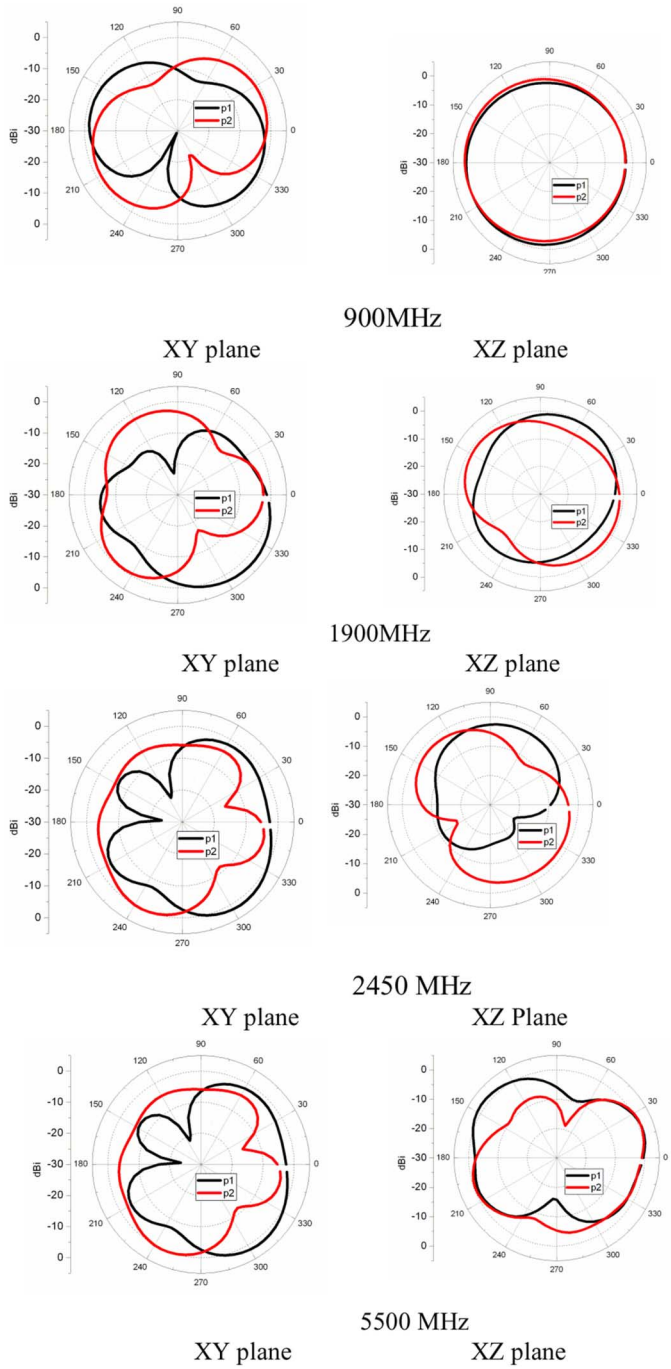

Fig. 8. Simulated radiation patterns at various frequencies when the two ports are excited, respectively.

and elliptical. These distributions can describe representative incoming polarized waves in elevation and/or azimuth. More complex measurement-based angular density functions can be found in [17].

It should be noted that the gain values include the total efficiency, which is affected by the coupling between elements. The MEG is normalized by a normalization of the gains as indicated in the equation [2]. The total efficiency of an antenna is defined in equation [1], as the total radiated power divided by the incident power at the feed. It includes reflection losses due

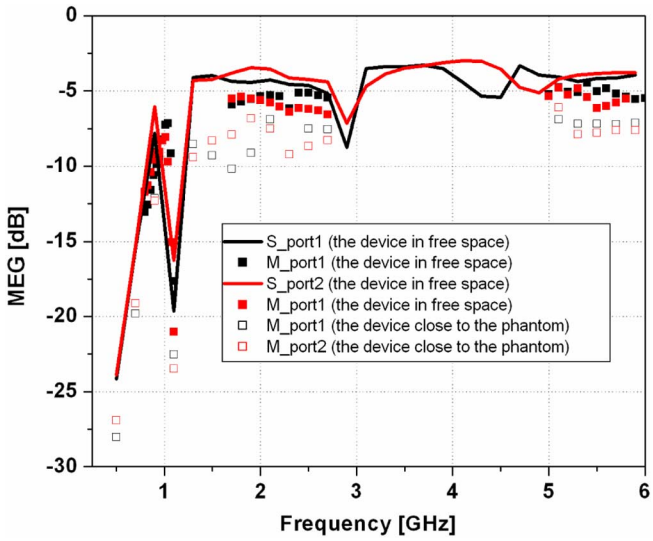

Fig. 9. Simulated (S) and measured (M) mean effective gain.

to the mismatch between the cable and the antenna, as well as dielectric and Ohmic losses. In multi-antenna systems, isolation is an additional factor to consider, because if any energy input at one antenna port can exit through another port, that energy will be dissipated in the terminal load of the second port, rather than contributing to useful radiation that can be intercepted remotely. Equations (3) and (4) can be used to compute the respective total efficiency of the two elements

$$\eta_{\text{total}1} = \eta_1(1 - |S_{21}|^2) \tag{3}$$

$$\eta_{\text{total}2} = \eta_2(1 - |S_{12}|^2). \tag{4}$$

Based on the above assumptions, the MEG was initially simulated and measured in a uniform channel, which corresponds to a 0 dB cross polarization ratio (XPR). The measured and simulated MEG results are shown in Fig. 9. It can be observed that the maximum discrepancy within the bandwidth of interest is approximately 2–3 dB, which is an acceptable difference, given the complex multiband design and tolerance variations between simulation and measurements. The two antennas achieve stable MEG values of about -5 dB at higher frequency bands, such as 1.5–2.8 GHz and 3–6 GHz. However the MEG is significantly lower at lower frequency bands, such as below 900 MHz. This is because the radiating structures of the antennas have smaller electrical size at the lower frequencies, and the separation is electrically smaller. At these low frequencies, the antennas suffer from low efficiency and higher coupling power loss. It can be seen that the ratio of MEG1, as determined at the port1, and MEG2, as determined at port2, are nearly 1.0 across all frequency bands. This means that the ports have met an equality requirement of a difference of less than 3 dB for the frequency bands of interest.

The ECC is another important parameter in the calculation of the diversity performance. Multiple methods of calculating the ECC are available: using far-field pattern data, and using

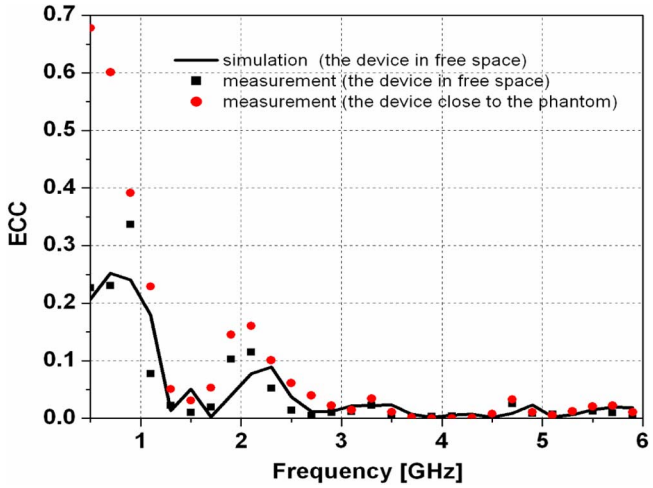

Fig. 10. Simulated and measured envelop correlation coefficient where $\mathrm{E}_{\theta n}(\theta, \varphi)$ is the θ polarized complex electric field radiation pattern of the antenna number n. Here, $n = 2$.

S-parameters [18]–[20]. A simplified form of the expression is written in [18] as

$$\rho_e = \frac{N}{D_1 D_2}$$
$$N = \left| \int_0^{2\pi} \int_0^{\pi} (\mathrm{XPR}\, E_{\theta 1}(\theta,\phi) E^*_{\theta 2}(\theta,\phi) P_\theta(\theta,\phi) + E_{\phi 1}(\theta,\phi) E^*_{\phi 2}(\theta,\phi) P_\phi(\theta,\phi)) \sin\theta\, d\theta d\phi \right|^2$$
$$D_1 = \left| \int_0^{2\pi} \int_0^{\pi} (\mathrm{XPR}\, E G_{\theta 1}(\theta,\phi) P_\theta(\theta,\phi) + G_{\phi 1}(\theta,\phi) P_\phi(\theta,\phi)) \sin\theta d\theta d\phi \right|$$
$$D_2 = \left| \int_0^{2\pi} \int_0^{\pi} (\mathrm{XPR}\, E G_{\theta 2}(\theta,\phi) P_\theta(\theta,\phi) + G_{\phi 2}(\theta,\phi) P_\phi(\theta,\phi)) \sin\theta d\theta d\phi \right| \quad (5)$$

Fig. 10 illustrates the simulated and measured ECC. The ECC has higher values at the lower frequencies than at the higher frequencies. The higher ECC is expected at the lower frequencies due to the small antenna separation.

Computation of the ECC, as described above, requires knowledge of the radiation pattern and involves integral calculation, which can be time-consuming to measure and calculate. To make this process easier, an alternate method for calculating the ECC from the *S*-parameters of the diversity antenna system has been derived [18]–[20]

$$\rho_e = \frac{|S^*_{11} S_{12} + S_{22} S^*_{21}|^2}{(1 - (|S^2_{11} + S^2_{12}|))\,(1 - (|S^2_{22} + S^2_{12}|))} \quad (6)$$

Fig. 11 illustrates the simulated ECC from the radiation patterns and *S*-parameters. The differently-calculated results have

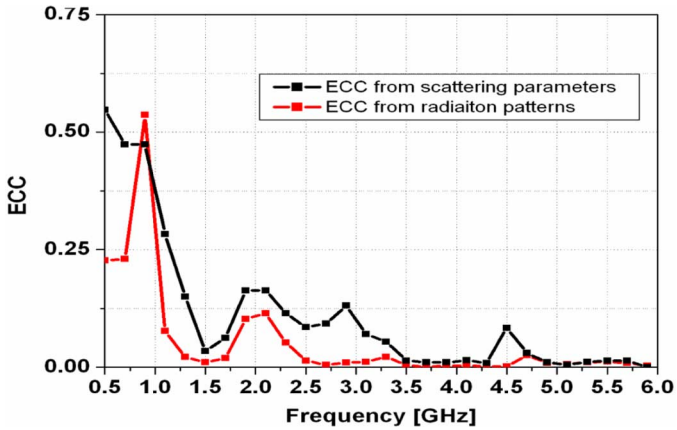

Fig. 11. Comparison of simulated ECC from radiation patterns and scattering parameters.

acceptable agreement at some frequencies, but significant discrepancies at other frequencies.

This situation can be explained: The ECC values in [6] are bounded simultaneously by three assumptions: 1) the antenna system is a lossless structure, 2) one antenna is excited while the other is terminated with a reference impedance (such as 50Ω); and 3) the antenna system is in a uniform scattering environment.

In the current simulations, the models are set to satisfy the second and third assumption: one antenna is excited and the other ends with the reference impedance (such as 50 Ω); and the antenna system is in a uniform scattering environment. However, for the first assumption, it is practically impossible due to unavoidable dielectric losses, conductor loss, mismatching loss and other sources of loss. However, if the antenna has a high port-to-port isolation and is well matched (low return loss), it is possible to maintain relatively stable reference impedance with low losses. This is why the ECC discrepancy between the two methods becomes smaller when the two antennas were well matched and had high isolation.

It should be noted that, although the third assumption has been recently confirmed by the diversity evaluation of several multi-antenna systems in different realistic propagation scenarios (e.g., uniform in the azimuth direction and Gaussian-like in elevation) and only small differences from uniform environments were noticed [21], [23], the third assumption is not always true. There are many on-line-of-sight (on-LoS) conditions over nonuniform channels and there are other research results that strongly indicate the contrary. For example, it has been argued and experimentally demonstrated that the scattering encountered in many suburban and rural environments is nonisotropic, that is, the distribution of angle of arrival (AoA) is not uniform. The use of a directional antenna with a nonuniform gain pattern at the receiver also results in nonisotropic power azimuth spectrum (PAS) as seen by the antenna [24]–[26].

All these limitations clearly demonstrate that, in a real antenna system, the ECC calculation from the scattering parameters does not give an exact value, but rather the lowest or the highest ECC value that can be reached.

TABLE I
CAPACITY AND DIVERSITY GAIN AT DISCRETE FREQUENCIES

UTA	Frequency [MHz]	Apparent diversity gain [dB]	Actual diversity gain [dB]	Capacity [bits/s/Hz]
DM-2-D	910	9.58333445	5.75091491	6.3802
	1900	10.0665896	8.67560137	8.0828
	2100	9.71516079	8.38383827	8.0836
	2600	10.0276578	8.59998049	8.0455
	5300	8.85172395	7.3892272	7.6182

Fig. 12. The two branch antenna was measured in a *RC* for diversity gain and capacity measurement.

D. Effect of a Nearby Human User on Antenna Diversity

The effect of a human user's head effects on antenna diversity is studied for the scenario of the mobile device. A user's head was simulated using a homogeneous SAM phantom and it consists of two layers of dielectric materials: a shell and a filling liquid. Specifications at several typical frequencies are below: For the shell, $\varepsilon_r = 5$, and $\sigma = 0.0125$ S/M was used for all frequencies, although brain tissue parameters vary over the operational frequency range. Typical tissue relative permittivity ε_r and conductivity σ at different frequency bands are recommended by IEEE or FCC. For example, $\varepsilon_r = 41.5$, and $\sigma = 0.97$ S/M for 900 MHz, $\varepsilon_r = 40$, and $\sigma = 1.4$ S/M for 1.8 GHz bands, and $\varepsilon_r = 39.5$ and $\sigma = 1.96$ S/M for 2.6 GHz.

MEG and ECC are tested in a uniform environment, respectively, when the device is nearby the head model. The results are plotted in Figs. 10 and 11 for comparison with the case without the phantom. It can be seen that the MEG is decreased across all frequency bands. This is because human head introduces absorption loss, which is higher at low frequencies. For the ECC, it is found that there is an increase in correlation at the low frequency band, in comparison to the free space case. This is due to the interaction between the antennas, phone chassis, and the head. The head alters both the magnitude and the phase of the radiation patterns, which may increase mutual coupling between the two antennas.

Specific absorption rate (SAR) was also evaluated at the three frequencies of 900, 1800, and 2600 MHz. The test system is called ALSAS-10U from APPREL [27]. In the simulation setup, the device is set at the touch position and the system ground plane is spaced 3.5 mm from the SAM phantom ear, and the central line of the mobile phone is oriented to have an angle of 60° with the vertical axis of the phantom head. For the test SAR values, the power levels delivered to an antenna port are all normalized to 24 dBm for 2600, 1800, and 900 MHz. The obtained SAR values are below. When the antenna operates at 900 MHz and closes to the right side of the phantom: 0.731 (port1) and 0.384 (port2). Similarly, for left side: 0.691 (port1) and 0.327 (port2). When the antennas operates at 1900 MHz, right side: 0.629 (port1) and 0.490 (port2), left side: 0.420 (port1) and 0.714 (port2); when the antennas operate at 2600 MHz, right side: 0.674 (port1), 1.242 (port2), left: 0.642 (port1), 0.890 (port2). It can be seen that all values are well below the SAR limit of 1.6 mW/g for practical applications. The differences in the SAR values between the left and right sides of the head are due to the asymmetrical placement of the antennas within the device.

E. Measurement of Diversity Gain and Capacity

We have measurement data for diversity gain and capacity of the two branch antenna systems from the Bluetest reverberation chamber (RC) of Chalmers Institute in Gothenburg, Sweden [28]. An RC is known to reproduce an isotropic uniform multipath environment. The measurement setup is shown in Fig. 12.

Diversity Gain: Both actual and apparent diversity gains are presented. The actual diversity gain gives a gain relative to a single antenna idea antenna, i.e., with an efficiency of 100%. The apparent diversity gain compares the gain relative to the best of the diversity antennas. The diversity gains are given at the 1% probability level in the cumulative distribution functions.

Capacity: The 3×2 MIMO Capacity results are presented as bits/second/Hertz in Table I, in which the base antennas comprise three monopoles, along the X, Y, and Z axes, respectively. $\mathrm{SNR} = 15$ dB for all frequencies. Through all frequency bands, the discrepancy ranges between the 3×2 capacity limit and the practical capacity of a 3×2 two branch antenna; from 1 to 3 bits/s/Hz. The maximum discrepancy occurs at 910 MHz.

IV. CONCLUSION

This paper has demonstrated a novel multiband diversity antenna system for handheld devices in practical use conditions for a real-world smart-phone, which include near-field clutter and the effect of a human user in close proximity. The proposed

diversity antenna system consists of two branches of folded monopoles, one of which is terminated with a rectangular patch. Without the need to use multiple antennas for multiband application, but by only slightly tuning the width of the patch and without changing the overall size of the antenna, the major radiation element of the proposed diversity antenna can achieve multiband operation from 890 MHz to 6 GHz. This includes the bands commonly used by handheld cellular devices, such as GSM 900/1800/1900 MHz, UMTS2100 MHz, Bluetooth 2.45 MHz, LTE 2.1/2.7 GHz dual-bands, and WiFi 2.6 GHz/3.3–3.8 GHz bands, in addition to WLAN 2.4/5.5 GHz bands. The proposed antenna occupies a surprisingly compact volume, merely 7 mm $\times$ 15 mm $\times$ 7.5 mm. The proposed antenna significantly reduces the volume typically required by other multiband systems, thereby overcoming a long-standing obstacle to multiband operations in small wireless mobile terminals. Additionally, high flexible frequency ratio and tuning to a desired bandwidth can be accomplished merely by changing the width of the patch, drastically simplifying antenna adjustment, which typically occurs at a late stage of product design. This eases the overall design process by allowing the finalization of the antenna's physical dimensions earlier in the design process.

Diversity performance was evaluated by studying the fundamental characteristics of the antenna, such as mutual coupling, and also calculating MEG and ECC. We have confirmed that the dual-diversity elements can achieve the mutual coupling of lower than 10 dB at the lower frequency at GSM 890 MHz, and even better than 15–20 dB at the higher frequency bands. Low mutual coupling is due to careful arrangement of antenna radiation elements, especially for the reduced surface currents on the GP.

The ECC values of the dual-diversity elements are less than 0.7 across all frequency bands, or less than 0.5 and even less than 0.1 at higher frequency bands. The low ECC values are mainly due to excellent diversity features for low coupling or high isolation. Since the two folded strip radiation elements are arranged orthogonally each other, they can easily achieve excellent polarization diversity and pattern diversity. The low ECC enables retention of enough signal independence between the received signals to effectively mitigate fading problems in real world MIMO multichannel propagation environments. When the antenna operates at the low frequency bands, the ECC increases, which is similar to diversity antenna systems based on conventional elements. However, when the device is in close proximity to a user's head, ECC increases at lower frequencies, rather than decreasing. This is a notable difference from many other diversity antenna systems. Two evaluation merits on ECC by *S*-parameters and by radiation patterns are also compared for the proposed design, and the bounded conditions of ECC based on *S*-parameters are described in detail.

Each element of a dual-element diversity antenna has achieved acceptable MEG at low frequency bands below 1 GHz. When the device is in close proximity to a user's head, the MEG is significantly decreased at low frequency bands, due to power absorption by human body. This is similar to other available antenna systems.

Since SAR is of significant concern, the SAR performance of the dual-element antenna was also evaluated. Test results indicate that each port of a dual-element diversity antenna satisfies current SAR standards. This is likely due to weaker current distributions on the GP. Thus, desirable SAR performance can be obtained when the dual-diversity elements are set up at the bottom end of the handheld device away from a human head. Also, measurement results for the diversity gain and capacity of the antenna are shown, using results from a Bluetest RC.

REFERENCES

[1] J. N. Pierce and S. Stein, "Multiple diversity with non independent fading," *IRE Proc.*, pp. 89–104, Jan. 1960.

[2] W. C. Jakes, Jr., *Microwave Mobile Communications*. New York: Wiley, 1974.

[3] W. C. Y. Lee, *Mobile Communications Engineering*. New York: Wiley, 1982.

[4] R. G. Vaughan, "Signals in mobile communications: A review," *IEEE Trans. Veh. Technol.*, vol. 35, no. 4, pp. 133–145, Nov. 1986.

[5] R. G. Vaughan and J. B. Andersen, "Antenna diversity in mobile communications," *IEEE Trans. Veh. Technol.*, vol. 36, no. 4, pp. 149–172, Nov. 1987.

[6] R. G. Vaughan, "Polarization diversity in mobile communications," *IEEE Trans. Veh. Technol.*, vol. 39, no. 3, pp. 177–186, Aug. 1990.

[7] J. Lemieux, M. S. El-Tanany, and H. M. Hafez, "Experimental evaluation of space/frequency/polarization diversity in the indoor wireless channel," *IEEE Trans. Veh. Technol.*, vol. 40, no. 3, pp. 569–573, Aug. 1991.

[8] K. Ogawa and T. Uwano, "A diversity antenna for very small 800-MHz band portable telephones," *IEEE Trans. Antennas Propagat.*, vol. 42, no. 9, pp. 1342–1345, Sep. 1994.

[9] M. A. Jensen and Y. Rahmat-Samii, "Performance analysis of antennas for hand-held transceivers using FDTD," *IEEE Trans. Antennas Propagat.*, vol. 42, no. 8, pp. 1106–1113, Aug. 1994.

[10] J. S. Colburn, Y. Rahmat-Samii, M. A. Jensen, and G. J. Pottie, "Evaluation of personal communications dual antenna handset diversity performance," *IEEE Trans. Veh. Technol.*, vol. 37, pp. 737–746, Aug. 1998.

[11] Q. Rao and D. Wang, "Multiple input, multiple output antenna for handheld communication devices," U.S. Patent Appl. 20100194642.

[12] W. Geyi, Q. Rao, S. Ali, and D. Wang, "Handset antenna design: Practice and theory," *Prog. Electromagn. Res.*, vol. PIER 80, pp. 123–160, 2008.

[13] Q. Rao, S. Ali, and D. Wang, "Compact 3-D monopole antenna for potential 700 MHz band applications in handheld devices," U.S. Patent Appl. 33246.

[14] CST. 2008 [Online]. Available: http:/www.CST.com

[15] GEMS. [Online]. Available: http:/www.CST.com

[16] Satimo. [Online]. Available: http://www.satimo.com

[17] T. Taga, "Analysis for mean effective gain of mobile antennas in land mobile radio environments," *IEEE Trans. Veh. Technol.*, vol. 39, no. 2, pp. 117–131, 1990.

[18] S. Stein, "On cross coupling in multiple-beam antennas," *IRE Trans. Antennas Propagat.*, vol. 10, no. 5, pp. 548–557, Sep. 1962.

[19] Salonen and P. Vainikainen, "Estimation of signal correlation in antenna arrays," in *JINA Int. Symp. Ant.*, Nice, France, 2002, vol. 2, pp. 383–386.

[20] C. Blanch, J. Romeu, and I. Corbella, "Exact representation of antenna system diversity performance from input parameter description," *Electron. Lett.*, vol. 39, no. 9, pp. 705–707, May 2003.

[21] C. Di Nall, "Estimation of multiple antennas correction from S-parameters and efficiency measurements," presented at the COST 273, Bologna, Italy, Jan. 19–21, 2005.

[22] I. Salonen and P. Vainikainen, "Estimation of signal correlation in antenna array," in *Proc. JINA*, Nice, France, Nov. 2002, vol. 2, pp. 383–386.

[23] Z. Ying, V. Plicanic, T. Bolin, G. Kristensson, and A. Derneryd, "Characterization of multi-channel antenna performance for mobile terminal by using near field and far field parameters," presented at the COST 273, Goteborg, Sweden, Jan. 7–9, 2004.

[24] H. S. Rad and S. Gazor, "The impact of non-isotropic scattering and directional antennas on MIMO multicarrier mobile communication channels," *IEEE Trans. Commun.*, vol. 56, no. 4, pp. 642–652, Apr. 2008.

[25] R. Iqbal and T. D. Abhayapala, "On statistics of the mobile Rayleigh fading channel in non-isotropic scattering environments," in *Proc. IEEE Int. Symp. Commun. Inf. Tech.*, Oct. 2007, pp. 814–818.

[26] R. Iqbal, T. D. Abhayapala, and T. A. Lamahewa, "Generalised Clarke model for mobile-radio reception," *IET Commun.*, vol. 3, no. 4, pp. 644–654, 2009.
[27] ALSAS-10U. APPREL [Online]. Available: http://www.aprel.com
[28] RC. Chalmers Inst., Gothenburg, Sweden [Online]. Available: http://www.bluetest.se

Qinjiang Rao was born in Hubei, China. He received the M.S. degree in University of Electronic Science and Technology of China, in 1989, the Ph.D. degree from Peking University, in 1999, both in electrical engineering.

He joined Research in Motion (RIM) in July 2006 and currently serves as a Senior Technical Staff member of Advanced Technology. He is presently working on projects that focus on multiple antenna design for LTE/MIMO and diversity application for handheld devices. He has over 20 years of R&D experience in elecromagnetics and antennas in Canada, Japan, and China. His fields of study include high-frequency electromagnetic radiation, scattering and propagation, compact high-gain multipolarized base station antennas, electrically small antennas, ultra-broad/multiband antennas, and multifed diversity handheld antennas. He has published over 70 peer reviewed technical papers and holds more than 10 patents, others pending. He is also a reviewer of well-respected technical journals.

Dr. Rao received an interesting presentation prize in IWPC (International Wireless Industry Consortium) at Copenhagen Workshop, Oct., 2009, for his talk on MIMO antenna design for small handheld devices.

Kelce Wilson received the Ph.D. degree in electrical engineering, an MBA, a Juris Doctor law degree, and is registered as a patent practitioner with the US PTO.

He is a patent attorney with licensing, litigation, and prosecution experience in the field of mobile phone technology. He began his engineering career in the U.S. Air Force in 1989, and has worked in satellite control, radar, stealth aircraft, and computer security. In 2001, he began attending Capital University Law School to transition to a career in patent law. He worked in private at law firms, and joined RIM in 2008 to assist with licensing and patent prosecution. While at RIM, he became involved in litigation and patent acquisition. He currently leads a team of attorneys and engineers doing patent litigation, acquisition, and licensing.